ELSEVIER

Journal of Nuclear Materials 278 (2000) 202–206

journal of nuclear materials

www.elsevier.nl/locate/jnucmat

# Diffusion under irradiation of rare earth elements in apatite

P. Martin [a,*], A. Chevarier [a], G. Panczer [b]

[a] *Institut de Physique Nucléaire de Lyon, UMR 5822, IN2P3-CNRS, Université Claude Bernard Lyon1, 43 Bvd. du 11 Novembre 1918, F-69622 Villeurbanne cedex, France*

[b] *Laboratoire Physico-chimie des matériaux luminescents, UMR 5620 CNRS, Université Claude Bernard Lyon1, 43 Bvd. du 11 Novembre 1918, F-69622 Villeurbanne cedex, France*

Received 20 July 1999; accepted 1 October 1999

**Abstract**

Nuclear waste ceramic forms among which the apatite, are under development as an alternative to waste glass in case of selective confinement. In that context, we studied the diffusion of lanthanide ions ($La^{3+}$, $Eu^{3+}$) in hydroxyapatite over a temperature range of storage interest, taking into account a possible enhanced diffusion due to irradiation effects. The lanthanide ions are introduced in apatite targets using ion implantation. The diffusion coefficients are deduced from Rutherford backscattering spectroscopy (RBS) at each step of annealing and irradiation procedure. Evidence of enhanced diffusion is shown and can be explained as a diffusion process governed by defect migration towards the surface. Time resolved laser-induced fluorescence measurements show that, during enhanced diffusion performed under vacuum, the europium ions substitute the calcium ions preferentially in Ca(I) hydroxyapatite sites. 

## 1. Introduction

Apatites are potentially valuable inertial matrices to actinide and some long-lived fission product confinement [1]. Moreover, hydroxyapatite is formed as waste ashes from nuclear fuel reprocessing are incorporated in cement [2]. In this process hydroxyapatite becomes part of the waste matrix. The general formula for apatite is $Ca_{I0}(PO_4)_6X_2$, X being a fluorine, chlorine ion or a hydroxyl group. The crystal structure of apatite (space group $P6_{3/m}$) permits a wide range of cation and anion substitutions [3–5]. In particular the two calcium positions have distinct stereochemistries (Ca(I) with $C_3$ symmetry surrounded by nine oxygen and Ca(II) with $C_S$ symmetry surrounded by six oxygen and one ($OH^-$) ion [6,7]). They can accommodate a variety of univalent, divalent and trivalent cations as substituents [8].

The purpose of this work is to study diffusion of lanthanum and europium enhanced by alpha radioactivity environment. Lanthanum has been chosen as representative of a major yield fission product. Europium is representative of actinides as the chemical properties of $Eu^{3+}$ are very similar to those of trivalent actinides and in particular to $Am^{3+}$. Furthermore, $Eu^{3+}$ can be used as a local structural probe [9]. Implantation is used to introduce La and Eu ions into apatite. During the annealing procedure, the samples are irradiated by bismuth ions having an energy of 100 keV. These 100 keV Bi ions are representative of recoil nuclei resulting from actinide alpha radioactivity. They are known to produce a large atomic displacement rate [10]. Diffusion data are deduced from Rutherford backscattering spectroscopy (RBS) measurements and are analyzed through a diffusion model [11]. These results are discussed together with structural data obtained by time resolved luminescence spectroscopy.

## 2. Diffusion measurements

### 2.1. Experimental

Synthetic microcrystalline hydroxyapatite referenced as DNA Grade Biogel HTP was stacked into pellets at 0.4 GPa. The high crystallinity of the sample was

* Corresponding author.

0022-3115/00/$ - see front matter 
PII: S0022-3115(99)00254-8

confirmed by X-ray diffraction. Observation using scanning electron microscopy shows regular crystal sizes ($60 \times 20$ nm) with typical prism-shaped morphology of hydroxyapatite [12], this morphology implies a high density of grain boundaries with a mean diameter less than 10 nm.

Hydroxyapatite was implanted with 30 keV $La^+$ or $Eu^+$ ions at room temperature using the IPNL separator. The nominal dose was of $5 \times 10^{15}$ at./cm$^2$ corresponding to a maximum La or Eu concentration of 4 at.%. Four series of implanted samples were then submitted to successive 100 keV $Bi^{2+}$ irradiation, the annealing temperature being, respectively, set to 25°C, 150°C, 300°C and 500°C. It should be noticed that the bismuth ion range in the apatite pellets is equal to 40 nm, which is much larger than the depth range corresponding to the lanthanum distribution (16 nm); thus there is no overlap between the two distributions. In order to understand the influence of the irradiation flux, the $Bi^{2+}$ beam intensity was kept constant and equal to 5, 10 and 20 μA. Irradiation time was set in order to lead to cumulative doses ranging between $2.5 \times 10^{15}$ and $7.5 \times 10^{15}$ at./cm$^2$. The sputtering yield for Bi bombardment was estimated using the SRIM code [13] and leads to a sputter loss of 10 nm for a $7.5 \times 10^{15}$ at./cm$^2$ bismuth dose. At each step of the procedure, RBS analysis was performed allowing measurements of lanthanum profiles as a function of annealing and bombardment conditions.

### 2.2. Analysis

Lanthanum profiles deduced from RBS measurements are shown in Fig. 1 for an annealing temperature of 150°C and for different Bismuth doses. We noticed no loss of lanthanum ions in the samples, showing that sputtering due to the bombardment does not influence the diffusion process. However, a slight shift of the overall lanthanum distribution was observed which can be explained by the unidirectional beam bombardment. These distributions are analyzed on the basis of a model derived from Fick's second Law [11]

$$\frac{\partial C(x,t)}{\partial t} = \frac{\partial}{\partial x}\left(D\frac{\partial C(x,t)}{\partial x}\right) - v\frac{\partial C(x,t)}{\partial x}, \tag{1}$$

where $C(x,t)$ is the lanthanum concentration, $D$ the diffusion coefficient and $v$ is the drift velocity related to the driving force $f$ by the Nernst relation

$$v = \frac{fD}{kT}, \tag{2}$$

where $k$ is Boltzmann's constant. Eq. (1) is solved using a numerical procedure based on finite differences which allows to reproduce the lanthanum profile evolution. This approach is fully described in Cranck's book [14] and our implementation is based on the NAG FORTRAN library routine [15]. The diffusion coefficient values are deduced from the fit optimization.

Results are presented in Fig. 2. In the 25–500°C temperature range, irradiation-enhanced diffusion coefficients are nearly independent on temperature, they depend only on the bismuth beam intensity. In a previous work, Martin et al. [16] have studied thermal diffusivity of lanthanum and europium in hydroxyapatite, they determined an activation energy and a pre-exponential factor in the 400–600°C temperature range: 1.3 eV/at. and $1.3 \times 10^{-7}$ cm$^2$/s leading to diffusion coefficient values of $2.35 \times 10^{-17}$ cm$^2$/s at 400°C and $2.7 \times 10^{-15}$ cm$^2$/s at 500°C. In order to compare thermal and irradiation-enhanced diffusion we report the data obtained by Martin et al. in Fig. 2, showing that in our experimental conditions the part of thermal diffusivity is negligible.

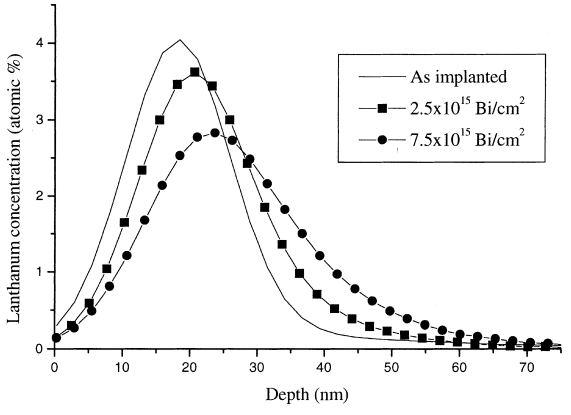


Fig. 1. Lanthanum profiles deduced from RBS measurements in case of 150°C annealing and after bismuth bombardment at different doses.

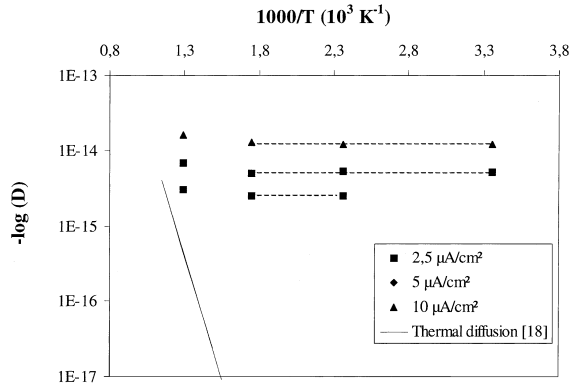


Fig. 2. Measured La diffusion coefficient vs. temperature, for different bismuth beam intensities.

During bismuth irradiation, vacancies and interstitials are created at a constant rate and are mobile, thus they can anneal out by various mechanisms, such as migration to internal or external surfaces, direct vacancies–interstitials annihilation, etc. These processes result in a steady-state concentration of defects in excess of the thermodynamic concentration characteristic of the working temperature. Dienes et al. [17] have treated the different annealing mechanisms and they have shown that one can easily identify the process that governs radiation-enhanced diffusion by representing the diffusion coefficient versus annealing temperature. In our case, the behavior is typical of a radiation-enhanced diffusion governed by defect annihilation at the surfaces or grain boundaries, it is due to the fact that the irradiation rate is strong enough to prevent spontaneous vacancy–interstitial recombination.

Radiation-enhanced diffusion is described by the formalism of Dienes et al. [17], the equations are simplified as there is no vacancy–interstitial spontaneous recombination

$$\begin{aligned}\frac{\partial C_{\mathrm{vac}}}{\partial t} &= \frac{\partial}{\partial x}\left(D_{\mathrm{vac}}\frac{\partial C_{\mathrm{vac}}}{\partial x}\right) + P(x) - K_{\mathrm{vac}}\left(C_{\mathrm{vac}} - C_{\mathrm{vac}}^{\mathrm{th}}\right),\\ \frac{\partial C_{\mathrm{int}}}{\partial t} &= \frac{\partial}{\partial x}\left(D_{\mathrm{int}}\frac{\partial C_{\mathrm{int}}}{\partial x}\right) + P(x) - K_{\mathrm{int}}\cdot C_{\mathrm{int}},\end{aligned} \tag{3}$$

$$D^{*} = D_{\mathrm{vac}}\cdot C_{\mathrm{vac}} + D_{\mathrm{int}}\cdot C_{\mathrm{int}}. \tag{4}$$

$C_{\mathrm{vac}}$ and $C_{\mathrm{int}}$ are the total atomic fractions of vacancies and interstitials, $C_{\mathrm{vac}}^{\mathrm{th}}$ is the atomic fraction of vacancy due to thermal annealing only, $P(x)$ is the production rate of vacancy–interstitial pairs, $K_{\mathrm{vac}}$ and $K_{\mathrm{int}}$ the characteristic proportionality constants for the rate of defects removal, $D_{\mathrm{vac}}$ and $D_{\mathrm{int}}$ the diffusion coefficients for vacancies and interstitials, $D^{*}$ the enhanced atomic diffusion coefficient.

Under steady-state condition, Eq. (3) reduces to [11]

$$\begin{aligned}\frac{\partial C_{\mathrm{vac}}}{\partial t} &= P(x) - K_{\mathrm{vac}}\left(C_{\mathrm{vac}} - C_{\mathrm{vac}}^{\mathrm{th}}\right) = 0,\\ \frac{\partial C_{\mathrm{int}}}{\partial t} &= P(x) - K_{\mathrm{int}}\cdot C_{\mathrm{int}} = 0.\end{aligned} \tag{5}$$

The constants $K_{\mathrm{int}}$ and $K_{\mathrm{vac}}$ are given by the relation (6)

$$\begin{aligned}K_{\mathrm{vac}} &= \alpha_{\mathrm{vac}} v_{\mathrm{vac}} \lambda_{\mathrm{vac}}^{2},\\ K_{\mathrm{int}} &= \alpha_{\mathrm{int}} v_{\mathrm{int}} \lambda_{\mathrm{int}}^{2},\end{aligned} \tag{6}$$

where $v_{\mathrm{vac}}$ and $v_{\mathrm{int}}$ are the effective jump frequencies for vacancies and interstitials, $\lambda_{\mathrm{vac}}$ and $\lambda_{\mathrm{int}}$ the jump distances for vacancies and interstitials, $\alpha_{\mathrm{int}}$ and $\alpha_{\mathrm{vac}}$ the proportionality constants. The diffusion coefficients are also expressed as a function of jump frequencies and jump distances by the following relations:

$$\begin{aligned}D_{\mathrm{vac}} &= C_{\mathrm{vac}} v_{\mathrm{vac}} \lambda_{\mathrm{vac}}^{2},\\ D_{\mathrm{int}} &= C_{\mathrm{int}} v_{\mathrm{int}} \lambda_{\mathrm{int}}^{2}.\end{aligned} \tag{7}$$

From Eqs. (5)–(7), we obtained the expressions of the diffusion coefficients

$$\begin{aligned}D_{\mathrm{vac}} &= \frac{P(x)}{\alpha_{\mathrm{vac}}} + C_{\mathrm{vac}}^{\mathrm{th}}\cdot v_{\mathrm{vac}}\cdot \lambda_{\mathrm{vac}}^{2},\\ D_{\mathrm{int}} &= \frac{P(x)}{\alpha_{\mathrm{int}}}.\end{aligned} \tag{8}$$

As the thermal diffusion coefficient [18] ($C_{\mathrm{vac}}^{\mathrm{th}} v_{\mathrm{vac}} \lambda_{\mathrm{vac}}^{2}$) is negligible compared to enhanced diffusion, we see from Eq. (8) that $D_{\mathrm{vac}}$ and $D_{\mathrm{int}}$ are temperature independent. The increased vacancy concentration due to the irradiation causes a proportional increase in diffusion by annihilation mechanism. The measured diffusion coefficient indeed seems to be proportional to the beam intensity. Such behavior is observed in Fig. 2, where the measured diffusion coefficients are shown to be temperature independent and to vary linearly with bismuth beam intensity

$$\begin{aligned}D_{I=2.5\ \mu\mathrm{A}} &= (2.5\pm 0.2)\times 10^{-15}\ \mathrm{cm}^{2}/\mathrm{s},\\ D_{I=5\ \mu\mathrm{A}} &= (5.2\pm 0.7)\times 10^{-15}\ \mathrm{cm}^{2}/\mathrm{s},\\ D_{I=7.5\ \mu\mathrm{A}} &= (1.2\pm 0.1)\times 10^{-14}\ \mathrm{cm}^{2}/\mathrm{s}.\end{aligned}$$

Martin et al. [16] have indeed observed that under thermal conditions all the lanthanide ions occupy substitutional calcium sites in hydroxyapatite. Then, the arising question is whether such an enhanced migration is connected either with lanthanide ion substitution in calcium sites or with grain boundary diffusion.

## 3. Europium location

Trivalent europium ions are widely used as luminescent probes in the investigation of the crystallographic structure of the activator centers in apatite [6]. The $^{5}D_{0} \rightarrow {}^{7}F_{0}, {}^{7}F_{1}, {}^{7}F_{2}$ transitions since $Eu^{3+}$ induces specific changes in the emission line, while the relative intensity is characteristic of the local symmetry [19].

### 3.1. Experimental

A pulsed nitrogen laser (Molectron, $\lambda_{\mathrm{exc}}$: 337 nm) was used as an excitation source. The spectral analysis of the luminescence was achieved at room temperature, by a MS 125 Oriel monochromator (400 and 1200 lines/mm gratings) and an intensified CCD detector (LOT-ORIEL MSTASPEC V) coupled with a delay generator (Stanford RS DG535) enabling time-resolving spectra acquisition. Long decay emissions of $Eu^{3+}$ ions were recorded with a delay of 1 μs and a gate width of 2 ms while short

decay emissions of $Eu^{2+}$ were recorded without delay and with a gate width of 100 ns.

### 3.2. Analysis

The emission spectra of the as-implanted pellet shows the characteristic bands of $Eu^{3+}$. They correspond to two sets of $Eu^{3+}$ transitions, $^5D_0 \rightarrow {}^7F_0, {}^7F_1, {}^7F_2$ related to Ca(II) (574, 629 nm) and Ca(I) positions (578, 591 and 617 nm) [9]. In Fig. 3, we observe that after bombardment, the first set related to Ca(II) substitutions disappears while the second one, related to Ca(I) substitution, remains. The emission intensity of $Eu^{3+}$ in a Ca(I) position increases regularly with the Bi dose, but over $10^{16}$ Bi/cm$^2$ the emission is unfortunately unobserved due to ablation effect. Along with these data, the short decay emission ($\tau = 600$ ns) of $Eu^{2+}$ is observed as a broad weak band (425–460 nm). It follows a similar evolution to that of $Eu^{3+}$ but, in this case, the Ca(I) and Ca(II) contributions could not be resolved.

## 4. Discussion

Evidence of lanthanum ion irradiation-enhanced diffusion with a 100 keV bismuth beam has been shown. It can be explained as a diffusion process governed by a defect migration towards both internal and external surfaces. Evidence of irradiation-enhanced diffusion has been obtained for bismuth doses lower than $10^{16}$ at./cm$^2$. In such conditions, the surface sputtering phenomenon does not affect the lanthanum profile. In order to know if bismuth irradiation leads to amorphization in the sample, we performed small angle X-ray diffraction at an angle of 0.4° from the surface. Such an angle leads to a depth analysis of 110 nm [18], which is less than the bismuth range in the sample, thus guaranteeing that the probed area has been irradiated. We used irradiation doses up to $10^{16}$ bismuth/cm$^2$. As we can see in Fig. 4, no modification of the X-ray spectrum was observed which shows that amorphization of the apatite lattice is negligible. This result is confirmed by Ritter and Mark [20] who had observed that under α irradiation, defects are annealed very quickly in apatite.

In order to get information on possible substitution of lanthanide ion in the apatite lattice, time resolved laser-induced measurements have been performed using Eu-implanted ions as a probe. The weak emission of the Eu in as-implanted pellets indicates that the main part of the Eu ions is located in microcrystallite interstitial positions. However, a small amount of Eu ions is shown to occupy the substitutional sites, Ca(II) and Ca(I). Analysis of emission spectra obtained after Bi bombardment shows that the main mechanism is the diffusion of Eu ions from interstitials, as well as from Ca(II) substitutionnal positions, to the high-symmetry Ca(I) sites. This diffusion convergence to Ca(I) site is consistent with the fact that the bombardment was conducted under vacuum. The same behavior has been observed during Eu thermal doping under vacuum by Gaft et al. [9]. The $Ca^{2+} \rightarrow Eu^{3+}$ substitution can occur much more easily with charge compensation provided by vacancies, than in the case of Ca(II). Furthermore, the non-oxidizing atmosphere leads to the Eu partial reduction to $Eu^{2+}$ ions, which are located in Ca positions in the same way as $Eu^{3+}$ ions. However, the much broader emission band did not unable the determination of the kind of involved Ca site. According to our previous results [18] on thermal diffusion performed under air, the reducing or oxidizing environment appears to be the key parameter for the Eu diffusion and for its substitutional location inside the apatite structure.

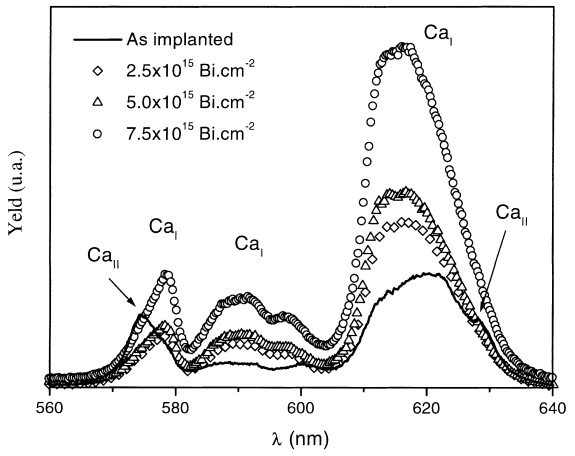


Fig. 3. Emission spectra of as Eu-implanted and of Bi-bombarded apatite ($\lambda_{exc} = 337$ nm)

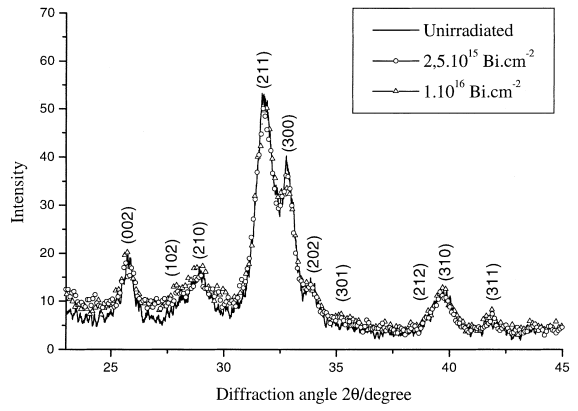


Fig. 4. Small angle X-ray diffraction spectra of hydroxyapatite in function of bismuth irradiation doses.

## 5. Conclusion

The goal of this work was not to reproduce as close as possible the possible nuclear storage conditions, but to give quantitative information on diffusion process that can occur in this context. Our longest irradiation time was 600 s which is equivalent to $2 \times 10^{21}$ $\alpha$ decays per gram which corresponds to 2000 yr of geological storage [18]. Furthermore, we made irradiation with a unidirectional beam which leads to a shift of the distribution. In the context of a migration barrier this effect cannot occur because $\alpha$ emission will be spatially independent. Hopefully, as explained in paragraph 2.2, the transport term $v$ has no influence on the value of the diffusion coefficient. The fact that diffusion coefficient is directly proportional to the simulated alpha radioactivity, we can easily extrapolate its value to the dose rate that will be expected, the value obtain is equal to $2 \times 10^{-23}$ cm$^2$/s which is very weak. Thus, hydroxyapatite appears to be a good candidate to migration barrier in nuclear waste storage.

## References

[1] J. Carpena, J.L. Lacout, French Patent No. 93 07265.
[2] E. Revertegat, G. Moine, Treatment and Conditioning of Radioactive Incinerator Ashes, Elsevier, London, 1991.
[3] M.E. Fleet, Y. Pan, J. Solid State Chem. 112 (1994) 78.
[4] M.E. Fleet, Y. Pan, Am. Mineral. 80 (1995) 329.
[5] M. Mikou, A. Taitai, J.L. Lacout, Ann. Chim. Fr. 10 (1985) 645.
[6] R. Jagannathan, M. Kottaisamy, J. Phys.: Condens. Matter. 7 (1995) 8453.
[7] R. Knubovets, Rev. Chem. Eng. 9 (1993) 161.
[8] J. Carpena, J.L. Lacout, Actual. Chim. 2 (1997) 3.
[9] M. Gaft, R. Reisfeld, G. Panczer, S. Shoval, B. Champagnon, G. Boulon, J. Lumin. 72–74 (1997) 572.
[10] R.C. Ewing, W.J. Weber, F.W. Clinard Jr., Prog. Nucl. Energy 29 (1995) 63.
[11] J. Philibert, Diffusion et transport de matières dans les solides, Les Éditions de Physique, Les Ulis, 1985.
[12] A. Ebrahimpour, M. Johnsson, C.F. Richardson, G.H. Nancollas, J. Colloid Interface Sci. 159 (1993) 158.
[13] J.F. Ziegler, J.P. Biersack, U. Littmark, The Stopping and Range of Ions in Solids, Pergamon, New York, 1996.
[14] J. Crank, The Mathematics of Diffusion, 2nd Ed., Clarendon, Oxford, 1975.
[15] NAGLIB Manual-FORTRAN, Mark 18, vol. 2, D03PCF, (1997).
[16] P. Martin, G. Carlot, A. Chevarier, C. Den Auwer, G. Panczer, J. Nucl. Mater. 275 (1999) 268.
[17] G.J. Dienes, A.C. Damask, J. Appl. Phys. 29 (1958) 1713.
[18] P. Martin, thesis, Lyon 1 University, 1999.
[19] M. Kottaisamy, R. Jagannathan, P. Jeyagpal, R.P. Rao, R.L. Narayan, J. Phys. D 27 (1994) 2210.
[20] W. Ritter, T.D. Mark, Nucl. Instrum. and Meth. B 1 (1984) 384.